ALK-PE

An efficient active learning Kriging approach for wave energy converter power matrix estimation

Ren, Chao; Tan, Jian; Xing, Yihan

DOI
10.1016/j.oceaneng.2023.115566

Publication date
2023

Document Version
Final published version

Published in
Ocean Engineering

Citation (APA)
Ren, C., Tan, J., & Xing, Y. (2023). ALK-PE: An efficient active learning Kriging approach for wave energy converter power matrix estimation. *Ocean Engineering*, *286*, Article 115566. https://doi.org/10.1016/j.oceaneng.2023.115566

Ocean Engineering 286 (2023) 115566

Contents lists available at ScienceDirect

Ocean Engineering

journal homepage: www.elsevier.com/locate/oceaneng

ALK-PE: An efficient active learning Kriging approach for wave energy converter power matrix estimation

Chao Ren [a], Jian Tan [b,*], Yihan Xing [a]

[a] Department of Mechanical and Structural Engineering and Materials Science, University of Stavanger, Norway
[b] Department of Maritime & Transport Technology, Delft University of Technology, The Netherlands

ARTICLE INFO

Keywords:
Active learning
Kriging surrogate model
Wave energy converter
WEC power matrix estimation

ABSTRACT

Wave energy is considered one of the most potential renewable energy. In the last two decades, many wave energy converters (WECs) have been designed to harvest energy from the ocean. Different power take-off systems are developed to maximize the power generation of WECs. However, the estimation of the power matrix of the WECs and annual power generation on the different sites is much more complex. A lot of simulations or experiments are required to obtain the power matrix of one specific WEC. To solve this problem, this paper proposes an active learning Kriging approach to estimate the WEC power matrix with less computational cost or experiment test. The efficiency of the proposed approach is demonstrated by two analytic problems and a point absorber WEC. The results show the proposed approach can efficiently and accurately estimate the power matrix of the WECs. Using the proposed ALK-PE approach, less than one-fifth of simulations or experiments are required to construct the whole power matrix of WECs at all the sea states, and the mean absolute percentage error is around 1%.

1. Introduction

Ocean wave energy is associated with plenty of merits. First, ocean waves carry a considerable amount of clean energy. The potential of global wave power is estimated to be in the order of 2 TW (Roberts et al., 2016). Secondly, ocean waves are a kind of continuous power input whether in the daytime or night, appealing to consumers. Thirdly, ocean wave energy is associated with good accessibility since most countries or regions have coasts. The history of our human beings attempting to exploit wave energy is long, and the first patent of utilizing wave energy can be traced back to more than two hundred years ago (Antonio, 2010). However, ocean wave energy is still characterized as an untapped energy resource. The exploitation of wave energy is limited compared with other renewable-energy technologies, such as offshore wind and solar energy (De Andres et al., 2017). One of the main reasons is that the economic performance of WECs is not satisfying (Astariz and Iglesias, 2015) since the estimated levelized cost of energy of WECs is clearly high. To accelerate the utilization of wave energy converters (WECs), it is of significance to optimize existing WEC concepts for driving down the levelized cost of energy.

As indicated in previous studies, the design and optimization of WECs appear to be site-dependent (O'connor et al., 2013; De Andres et al., 2016). This can be expected since the responses of the captor of WECs are affected by the wave inputs, including wave periods and wave heights. Thus, the distribution of occurrence of wave states could make a difference to the optimization results of WECs. The statistical information of wave resources is normally characterized as a form of scatter diagrams which consist of hundreds of cells to illustrate the probability of occurrence of each wave state. To assess the suitability of WECs for various sea sites, the power performance of WECs inherently has to be identified for a number of different wave states, which is then used to formulate a power matrix. Forming a power matrix is a prevalent way to reflect the power performance of WECs. In the power matrix, the power production of the device is depicted for a set of combinations of wave heights and wave periods. Properly evaluating the power performance of WECs is commonly time-demanding since the device has to be tuned to fit the variation of wave states. For instance, the power absorption of WECs is dependent on their power take-off (PTO) damping (Tan et al., 2021). To best reveal the potential of WECs, it is important to optimize the PTO damping for each wave state, where a large number of iterations are required. In addition, given the considerable number of wave states in scatter diagrams, obtaining a power matrix with a qualified resolution could even further increase the computational loads. Furthermore, the design of WECs normally needs to be optimized for being adapted to various sea sites. Correspondingly, the power matrix of WECs has also to be updated (Tan et al., 2022c). It can be expected that developing an efficient way to obtain the power

* Corresponding author.
E-mail address: tanjianmax@163.com (J. Tan).

https://doi.org/10.1016/j.oceaneng.2023.115566
Received 18 February 2023; Received in revised form 17 July 2023; Accepted 5 August 2023
Available online 16 August 2023

matrix of WECs is of great value to the design and optimization of WECs.

Numerical modeling can be used to analyze the performance of WECs at each wave state. The commonly-used numerical models in the context of WECs can be classified as computational fluid dynamics (CFD) modeling, frequency-domain modeling and time-domain modeling (Penalba Retes et al., 2015). In CFD models, the fundamental equations describing fluid dynamics, namely Navier–Stokes equations, are solved numerically. Thus, CFD modeling is inherently associated with high fidelity but its computational costs are considerable. For this reason, the application of CFD models in estimating the power performance of WECs is limited while they are mainly utilized in analyzing the survivability of WECs. Instead, frequency-domain and time-domain modeling are widely used to estimate the power performance of WECs, and both of them are established based on potential flow theory (Folley et al., 2012). Frequency-Domain modeling can be applied to reveal the frequency-dependent responses of harmonic motion efficiently, but all the concerned components have to be linear. Both frequency-domain modeling and time-domain modeling are established based on potential flow theory. Comparatively, time-domain modeling is applicable to cover the nonlinear force components, and the time-dependent responses of WECs can be described. Thus, time-domain modeling in principle has higher accuracy in power estimation, particularly for working regions with large displacement and velocity where nonlinearities are pronounced. For instance, it has been indicated in Folley et al. (2012) and Nielsen et al. (2018) that the accuracy of frequency-domain modeling is only limited to mild wave states. At the same time, nonlinear time-domain models present comparable results to the experiment in a wide range of operating conditions (Nielsen et al., 2018). However, in time-domain modeling, the partial differential equations must be solved numerically at each time step (Folley, 2016). The required computational time of time-domain modeling is typically several orders of magnitude higher than that of frequency-domain approaches (Tan et al., 2022a). Therefore, the use of time-domain modeling could make the whole design process of WECs time-consuming. A few recent studies have been dedicated to this challenge. As a result, some approaches have been proposed to cover nonlinear effects in an efficient manner. In Wei et al. (2019) and Mérigaud and Ringwood (2017), conventional frequency-domain modeling was extended to incorporate the nonlinear PTO force in the array of point absorbers. In Suchithra et al. (2019), a method to implement reduced-order time-domain modeling was proposed and validated for simulating point absorbers with hydraulic PTO systems. Alternatively, a relatively new modeling technique, namely spectral-domain modeling, was developed for WECs in Folley and Whittaker (2010). In spectral-domain modeling, the nonlinear force components can be represented by statistical linearization. Even though these alternative models contribute to improved accuracy with regard to linear models because of the inclusion of nonlinear components, their computational demands are still considerable for optimizing the WEC concepts where a large number of iterations are needed.

To reduce the computational cost, machine learning seems a better way to solve the problem. In the last two decades, many machine-learning models and tools have been developed, demonstrating an excellent power to solve engineering problems. Many researchers have applied ML tools and technologies to solve engineering problems. Zhou et al. (2022) combined physical modeling and deep neural network for the wind turbine power estimation. Stetco et al. (2019) summarized the machine learning methods for wind turbine condition monitoring. Hadi et al. (2022) applied deep reinforcement learning for adaptive path planning and control of an autonomous underwater vehicle. Ren et al. (2020) applied deep learning for the offshore wind turbine jacket stress prediction considering the corrosion effect. For the wave energy, Bento et al. (2021) used deep-learning neural networks for ocean wave energy forecasting. Lu et al. (2022) used a hybrid machine learning model to predict the short-term wave energy flux. Zhu et al. (2022) conducted a layout study of WECs using an artificial neural network. The results show that the ML models can make accurate predictions given enough data sets. However, in most studies, it requires a lot of simulations to train accurate ML models. Normally, the "One-shot" training approach is applied to construct the machine learning models. The training data are all generated in advance, and the machine learning model is trained and validated only once or a few times. To guarantee the accuracy of ML prediction, ten of thousands of training data (simulations) are generated. That will be much more time-consuming for the WEC numerical simulation and is inapplicable for the WEC power matrix estimation.

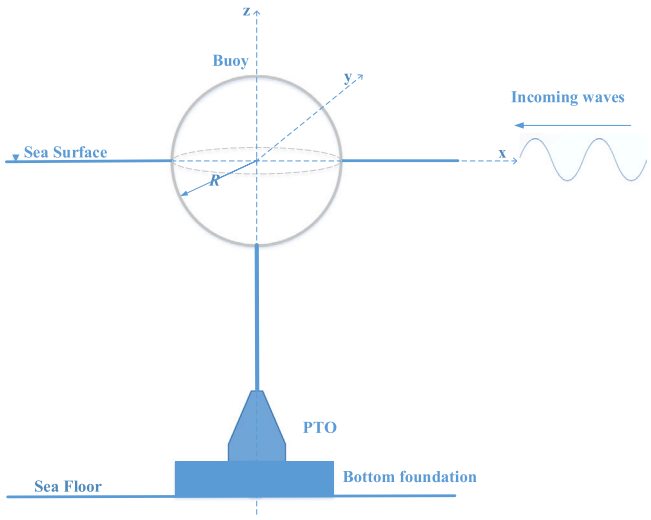

Fig. 1. Schematic of the spherical heaving point absorber with a bottom founded PTO.

Compared to the "One-shot" training approach, the active learning training strategies (Ren and Xing, 2023; Settles, 2009; Ren et al., 2022; Moustapha et al., 2022; Ren et al., 2023) are more efficient. The idea of active learning approaches is to train the ML models with a small data set at first. Then, it selects one or several sample points at each iteration to construct the machine learning models which are updated at each iteration efficiently until the convergence. Usually, the active learning approach needs less training data (simulations), which is more suitable for time-consuming simulation. Additionally, among all the machine learning models, the Gaussian process regression model (also named Kriging) is widely used with the active learning approach for the engineering problem. Ren (2022) applied the Kriging model with active learning approaches for wind turbine reliability assessment. Sarkar et al. (2016) also applied Kriging for the WEC array optimization. Both of the studies demonstrated the efficiency and accuracy of the active learning approaches. Therefore, this paper proposes an efficient WEC power matrix estimation approach using an active learning Kriging approach. A typical variance reduction learning approach is adopted to update the Kriging model. Also, a classic stopping criterion is applied to end the updating process. More details can be found in the following sections.

The layout of this paper is organized as follows. The WEC model, PTO system, and typical power estimation approach are given in Section 2. The overview of the active learning approach and the proposed ALK-PE approach are provided in Section 3. Also, two analytic problems are used to demonstrate the proposed approach. Section 4 applies the proposed approach to the WEC power estimation considering two different scenarios. At last, the conclusion and discussion are given in Section 5.

2. Wave energy converter model

2.1. The point absorber wave energy converter

This section describes the considered WEC concept. A generic heaving point absorber is used as the WEC reference in this study. The

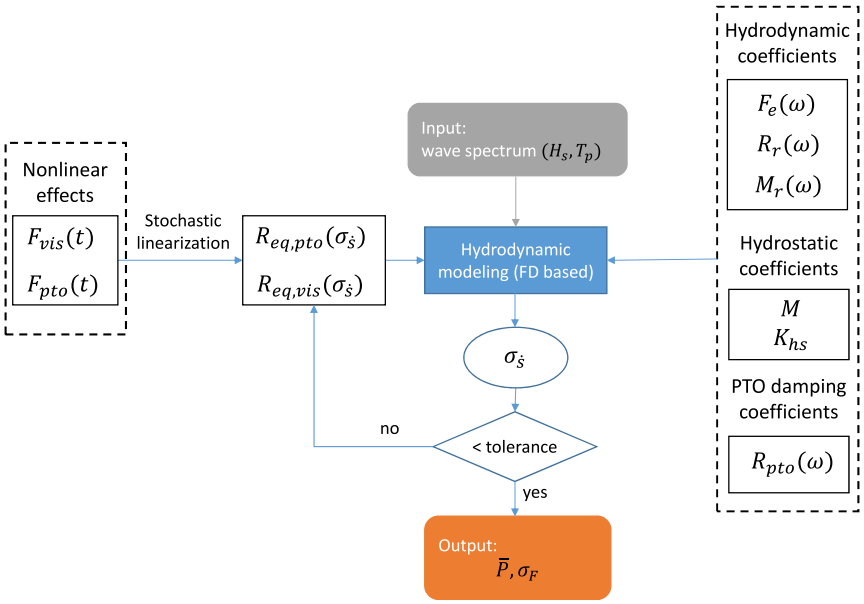

Fig. 2. The diagram of the SD model in estimating the performance of WECs.

schematic of the WEC is shown in Fig. 1. The geometry of the floating buoy is a sphere with a radius R of 2.50 m and the buoy is semi-submerged in still water. Given the water density of 1025 kg/m^3, the mass of the buoy is calculated as 33 543 kg according to Archimedes' principle. Besides, the operating condition is assumed to be deep water. The spherical buoy is connected to the moving part of the PTO, and the moving part could be a piston or generator translator depending on the PTO type. Furthermore, a passive control strategy is implemented for the studied point absorber, which implies that only a force proportional to the buoy velocity is applied by the PTO system (Tan et al., 2023a, 2020, 2022b).

2.2. Numerical modeling

In this work, a verified spectral-domain model is applied to predict the power performance of WECs. The model results are used as the data source as well as the reference to verify the proposed machine learning method. The formulation of the model is only briefly introduced here. More details and validation of the numerical model can be found in Tan et al. (2022a, 2023b). The diagram of the spectral-domain model is depicted in Fig. 2. In the model, the incoming waves are expressed based on the linear wave theory, and all the considered waves are assumed to be irregular and unidirectional. Under linear wave theory, irregular waves are reasonable to be represented by the superposition of a set of regular waves with random phases. The regular wave can be expressed as:

$$\eta(t) = \zeta_a \cos(\lambda x - \omega t) \tag{1}$$

where t is time, λ is the wave number, ω is the angular frequency of the incoming wave and ζ_a is the wave amplitude. Then, the irregular wave input can be expressed as

$$\eta(t) = \sum_{j=1}^{N} \zeta_a(\omega_j) \cos(\lambda(\omega_j)x - \omega_j t + \varphi(\omega_j)) \tag{2}$$

where $\lambda(\omega_j)$, $\zeta_a(\omega_j)$ and $\varphi(\omega_j)$ are the wave number, wave amplitude and phase of the regular wave component corresponding to the frequency component ω_j. Regarding irregular wave conditions, the JONSWAP spectrum together with peakedness factor of 3.3 is applied (Edition et al., 2001). For each wave state, 500 individual harmonic wave components with a random set of phases between frequency components are considered. The angular frequencies of the wave components are uniformly spaced from 0.1 to 4.0 rad/s.

In a predefined wave spectrum, the amplitude of the wave component is related to the wave energy spectrum S_{ζ_a}, as

$$\zeta_a(\omega_j) = \sqrt{2S_{\zeta_a}(\omega_j)\Delta\omega} \tag{3}$$

The variance of the wave elevation $\sigma^2_{\zeta a}$ is calculated as

$$\sigma^2_{\zeta a} = \sum_{j=1}^{N} S_{\zeta_a}(\omega_j)\Delta\omega \tag{4}$$

where $\sigma_{\zeta a}$ is the standard deviation (STD) of the wave elevation.

For a single rigid floating body subjected to ocean waves, its motion can be described based on Newton' second law as

$$M\ddot{s}(t) = F_{hs}(t) + F_e(t) + F_{pto}(t) + F_r(t) + F_{vis}(t), \tag{5}$$

where M represents the mass of the oscillating buoy, s is the buoy's displacement, F_{hs} is the hydrostatic force, F_e is the wave excitation force, F_r is the wave radiation force, F_{pto} is the PTO force, F_{vis} is the viscous drag force. In the spectral-domain approach, the motion of a floating body can also be characterized as the form of complex amplitudes since spectral-domain modeling is an extension of frequency-domain modeling. Thus (5) can be rewritten as

$$\hat{F}_e(\omega) = \hat{s}(\omega)\{\left[-\omega^2(M + M_r(\omega)) + K_{hs}\right] + \mathrm{i}\omega[R_r(\omega) + R_{pto,eq} + R_{vis,eq}]\} \tag{6}$$

where $R_r(\omega)$ is the radiation damping coefficient; ω is the angular wave frequency, $M_r(\omega)$ is the added mass of the buoy, $\hat{s}$ is complex amplitude of the displacement, and K_{hs} is the hydrostatic stiffness. $R_{pto,eq}$ and $R_{vis,eq}$ are equivalent linear PTO damping and equivalent linear viscous damping in spectral-domain modeling to represent two typical nonlinear effects, namely the PTO force saturation and viscous drag force. The PTO force saturation occurs when the PTO force is about to violate the designed force limit of the system. Thus, the PTO force in the time domain is expressed as

$$F_{pto}(t) = \begin{cases} -R_{pto}\dot{s}(t), & for \quad |R_{pto}\dot{s}(t)| \le F_m \\ \mathrm{sign}[-R_{pto}\dot{s}(t)]F_m, & for \quad |R_{pto}\dot{s}(t)| > F_m \end{cases} \tag{7}$$

where F_m represents the PTO force limit. The stochastic linearization of the nonlinear PTO force has been given in Folley and Whittaker (2010), Tan et al. (2022a), and it can be calculated as

$$R_{eq,pto} = \frac{2R_{pto}}{\sigma^3_{\dot{s}}\sqrt{2\pi}}\left[\frac{\sqrt{\pi}\sigma^3_{\dot{s}}\,\mathrm{erf}\left(\frac{u_1}{\sqrt{2}\sigma_{\dot{s}}}\right)}{\sqrt{2}} - \sigma^2_{\dot{s}}u_1\exp\left(\frac{-u_1^2}{2\sigma^2_{\dot{s}}}\right)\right]$$

$$+\frac{2R_{pto}u_1\sqrt{2\pi}}{\sigma_{\dot{s}}}\exp(\frac{-u_1^2}{2\sigma_{\dot{s}}^2}) \tag{8}$$

where R_{pto} is the actual PTO damping set for the system, $\sigma_{\dot{s}}$ is STD of the velocity, "erf" represents error function, and u_1 is the ratio between the PTO force limit and the PTO damping coefficient, expressed as

$$u_1 = \frac{F_m}{R_{pto}} \tag{9}$$

The viscous drag force is represented by a quadratic damping term which is similar to the drag component in Morison's equation (Edition et al., 2001), and in the time domain it can be expressed as

$$F_{vis} = -\frac{1}{2}\rho C_D A_D |\dot{s}|\dot{s} \tag{10}$$

where ρ is the water density, C_D is the drag coefficient, A_D is the characteristic area of the buoy, and $\boldsymbol{u_0}$ is the undisturbed flow velocity at the centroid of the buoy. Based on the investigation in Giorgi and Ringwood (2017), the drag coefficient is selected as 0.6 to minimize the error of the power estimate resulting from the viscous drag force. The linear equivalent viscous damping in spectral-domain modeling has been derived in Folley and Whittaker (2010, 2013), as

$$R_{vis,eq} = \frac{1}{2}\rho C_D A_D \sigma_{\dot{s}}\sqrt{\frac{8}{\pi}} \tag{11}$$

An iterative process is required to solve (6) since $\sigma_{\dot{s}}$ in the linear equivalent damping coefficients is unknown. In each iteration, the complex amplitude of the WEC at each frequency component can be obtained by solving (6). Then, the complex amplitude of the velocity is expressed as

$$\hat{\dot{s}}(\omega) = \omega\hat{s}(\omega) \tag{12}$$

the corresponding STD of the velocity can be expressed as

$$\sigma_{\dot{s}} = \sqrt{\sum_{j=1}^{N}\frac{|\hat{\dot{s}}(\omega_j)|^2}{2}} \tag{13}$$

In this work, the iteration continues until the difference between the previous and iterative value converges within 0.1%. Then, the mean absorbed power of the WEC at each wave state can be calculated as:

$$\overline{P} = R_{eq,pto}\sigma_{\dot{s}}^2 \tag{14}$$

The PTO damping plays an important role in the dynamics of WECs. The selection of the PTO damping coefficient could determine the power absorption of the WEC. To improve the power production of WECs, it is important to select the PTO damping coefficient for each wave state properly. In addition, the PTO force is strongly related to the PTO damping coefficient. The maximum PTO force should be considered as a constraint in the tuning of the PTO damping coefficient. Given the randomness of the wave inputs, the constraint can be characterized by the occurrence probability of the PTO force exceeding the maximum PTO force F_m. Considering Rayleigh distribution (Journée et al., 2015), the probability is calculated by

$$\beta(\sigma_F) = \exp(\frac{-F_m^2}{2\sigma_F^2}) \tag{15}$$

where σ_F represents STD of the PTO force, which can be related to the PTO damping as

$$\sigma_F = R_{eq,pto}\sigma_{\dot{s}} \tag{16}$$

In the present work, the "Interior-Point" algorithm in Matlab environment is applied, and the termination criterion of the function is defined as 1e–5. In the optimization, the tolerance on the probability of exceeding the PTO force limit is defined as 20%, referring to Tan et al. (2022a). The search bound is defined as $[0, 50R_r(\omega_p)]$, where ω_p represents the corresponding angular frequency of the concerned peak period of the wave state. To comprehensively illustrate the suitability of the AL method to power prediction of WECs, two different scenarios are set up. In the first case, there is no PTO force constraint while a PTO force limit of 80 kN is implemented in the second case.

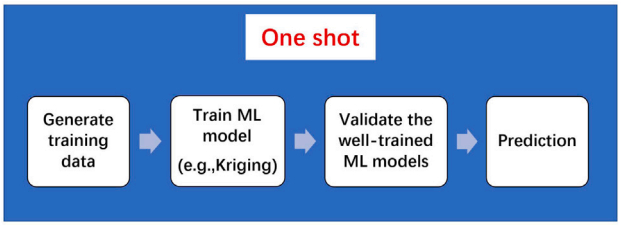

Fig. 3. One-shot training approach.

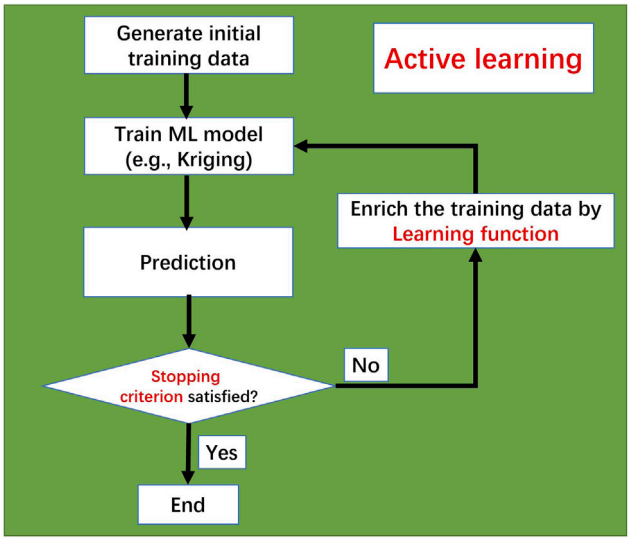

Fig. 4. Active learning training approach.

3. Active learning approaches and proposed ALK-PE approach

3.1. Active learning approaches

In this subsection, a brief introduction to active learning approaches is presented. As mentioned previously, the training strategies of machine learning models can be divided into (1). One-shot approach (as shown in Fig. 3) (2). Active learning approach (as shown in Fig. 4). The one-shot approach is now widely used to construct the data-driven model, which requires a lot of training data. Contrary to the one-shot approach, active learning at the beginning only requires a small training data set and then updating the ML models using the enriched sample selected by the learning function. The updating process will stop when the stopping criterion is satisfied. Therefore, the learning function and stopping criterion are the two most important factors for an active learning approach. They will directly affect the efficiency of the approach and the accuracy of ML model prediction. The learning function and stopping criterion are needed to be carefully designed. The learning function and stopping conditions of the proposed approach are given in the following subsection. A brief introduction to the Kriging model is also given in the next subsection.

3.2. Kriging model

The Kriging model, also known as Gaussian process, was first introduced by Krige (1951) in the field of geostatistics. It is based on the assumption that the response function consists of a regression model and a stochastic process, given by:

$$G(\mathbf{x}) = \mathbf{f}(\mathbf{x})^T\boldsymbol{\beta} + z(\mathbf{x}) \tag{17}$$

where $\mathbf{f}(\mathbf{x})$ is the basic function vector, $\boldsymbol{\beta}$ is the corresponding regression coefficient vector, and $z(\mathbf{x})$ represents a stationary Gaussian process with zero mean and the covariance between two points, $\mathbf{x_i}$ and $\mathbf{x_k}$:

$$\mathrm{cov}(z(\mathbf{x_i})z(\mathbf{x_k})) = \sigma^2 R_\theta(\mathbf{x_i}, \mathbf{x_k}) \tag{18}$$

where σ^2 and $R_\theta(\mathbf{x_i}, \mathbf{x_k})$ are respectively the process variance and a Gaussian correlation function defined by a vector of parameters θ. Several correlation functions are available for the Kriging model. In this paper, the typical squared exponential correlation function is applied which reads as:

$$R_\theta\left(\mathbf{x}_i, \mathbf{x}_k\right) = \prod_{j=1}^{n} \exp\left[-\theta_j \left(\mathrm{x_{i(j)}} - \mathrm{x_{k(j)}}\right)^2\right] \tag{19}$$

where $\mathrm{x_i^{(j)}}$ and $\mathrm{x_k^{(j)}}$ are the jth values of the vectors $\mathbf{x_i}$ and $\mathbf{x_k}$. θ_j is a scalar that gives the multiplicative inverse of the correlation length in the jth direction. The unknown parameters ($\boldsymbol{\beta}$, σ^2, θ) of the Kriging model can be optimized by maximum likelihood estimation. Once the optimal values of the three parameters are obtained, the expected value $\mu_{\hat{G}}$ and the variance $\sigma^2_{\hat{G}}$ at a point $\mathbf{x}$ can be determined by the equations:

$$\mu_{\hat{G}}(\mathbf{x}) = \beta + \mathbf{r}(\mathbf{x})\mathbf{R}_\theta^{-1}(\mathbf{Y} - \mathbf{1}\beta) \tag{20}$$

$$\sigma^2_{\hat{G}}(\mathbf{x}) = \sigma^2\left(1 + u(\mathbf{x})^T\left(\mathbf{1}^T\mathbf{R}_\theta^{-1}\mathbf{1}\right)^{-1}u(\mathbf{x}) - \mathbf{r}(\mathbf{x})^T\mathbf{R}_\theta^{-1}\mathbf{r}(\mathbf{x})\right) \tag{21}$$

where $\mathbf{r}(\mathbf{x}) = \left\{R\left(\mathbf{x}, \mathbf{x}_1\right), R\left(\mathbf{x}, \mathbf{x}_2\right), \ldots, R\left(\mathbf{x}, \mathbf{x}_n\right)\right\}$ represents the correlation vector between the unknown point $\mathbf{x}$ and n all known experimental points and $u(\mathbf{x})$ can be expressed as $u(\mathbf{x}) = \mathbf{1}^T\mathbf{R}_\theta^{-1}\mathbf{r}(\mathbf{x}) - 1$. The value $\mu_{\hat{G}}$ is always considered as the Kriging prediction value, and the value $\sigma_{\hat{G}}$ is the related predicted error. In this paper, the value $\mu_{\hat{G}}$ represents the predicted mean power value $\hat{\bar{P}}$, and the $\sigma_{\hat{G}}$ denotes the predicted error ($\sigma_{\hat{\bar{P}}}$) of the mean power prediction. Additionally, the $\sigma_{\hat{G}}$ value is easily obtained in most Kriging surrogate modeling toolboxes, e.g., the DACE toolbox (Lophaven et al., 2002) for MATLAB users and Scikit-learn toolbox (Pedregosa et al., 2011) for Python users.

3.3. Proposed ALK-PE method

In this subsection, the proposed approach is presented. The learning function and stopping criterion details are given. The general algorithm of the proposed approach is listed at the end.

3.3.1. Learning function

To get an accurate power matrix prediction of the WECs, it is better to reduce the prediction error ($\sigma_{\hat{\bar{P}}}$) of the mean power value at each sea state case. Therefore, the learning function must reduce the prediction error to get an accurate prediction. A typical error reduction learning approach will be used here, which gives:

$$i^* = \arg\max\left(\sigma_{\hat{\bar{P}}}\left(x_j\right)\right) \quad \text{where j} = 1, 2 \ldots \mathrm{M} \tag{22}$$

where i^* is the enriched sample number, M is the total number of all the unsimulated samples, and x_j represents the different combination samples of wave height and wave period. As the prediction error is easily obtained from the Kriging surrogate model, the learning function will select the sea state case (x_{i^*}) with the maximum prediction error. The newly selected wave case and the related simulated mean power value will be used to update the Kriging model.

3.3.2. Stopping conditions

To guarantee the ML prediction at each sea state, the typical U (Echard et al., 2011) function is adapted here named as UI function that can be used as a factor to ensure the prediction accuracy:

$$UI(\mathbf{x_j}) = \frac{\left|\hat{\bar{P}}(\mathbf{x_j})\right|}{\sigma_{\hat{\bar{P}}}(\mathbf{x_j})} \tag{23}$$

The $UI(\mathbf{x_j})$ denotes the inverse ratio between Kriging prediction error and prediction value at x_j. To end the active learning process and guarantee the accuracy of Kriging prediction at each sea state, the minimum value of $UI(\mathbf{x_j})$ should be greater than $\boldsymbol{\Phi}$

$$\min UI(\mathbf{x_j}) > \boldsymbol{\Phi} \tag{24}$$

where $\boldsymbol{\Phi}$ is the threshold of the stopping criterion. Different $\boldsymbol{\Phi}$ values will be tested in the following studies. With the learning function and stopping criterion, the general algorithm of the proposed approach can be formulated in Algorithm 1. X_{doe}, X_{all}, and $\bar{P}_{doe}$ are, respectively, the initial sea state data set, the whole sea state data set, and the initial simulated mean power.

Algorithm 1 ALK-PE: An efficient active learning Kriging approach for wave energy converter power matrix estimation

Input: X_{doe}, $\bar{P}_{doe}$, X_{All}

$N_{doe} \leftarrow m_i$ ▷ m_i is the number of initial training samples (design of experiments)

while $\min(UI) \le \boldsymbol{\Phi}$ **do**

1. Train the Kriging model with X_{doe} and $\bar{P}_{doe}$.
2. Get the Kriging prediction value ($\hat{\bar{P}}(x_j)$) and error ($\sigma_{\hat{\bar{P}}}(x_j)$) of the all the sea states (X_{All}).
3. Search x_{i^*} where $i^* = argmax(\sigma_{\hat{\bar{P}}}(x_j))$ and simulated the mean power $\bar{P}_{i^*}$.
4. Calculate the $UI(x_j)$ value based on $\hat{\bar{P}}(x_j)$ and $\sigma_{\hat{\bar{P}}}(x_j)$

$N_{doe} \leftarrow N_{doe} + 1$

$X_{doe} \leftarrow X_{doe} \cup x_{i^*}$

$\bar{P}_{doe} \leftarrow \bar{P}_{doe} \cup \bar{P}_{i^*}$

end while

Output: Predicted mean power $\hat{\bar{P}}$ of all the sea states (X_{All}).

3.4. Demonstration for analytic examples

In this subsection, two analytic examples are used to demonstrate the proposed ALK-PE approach. The first one is a one-dimension problem, and the second one is a two-dimension problem. In these two examples, the wave converter power matrix is assumed as an explicit function of the variables. However, the wave converter power matrix can hardly be expressed as an explicit function in reality. These two analytic problems are merely used as simple examples to help readers to understand the proposed approach and calibrate the convergence criterion. Additionally, the two examples are easy to repeat and do not require a long-time simulation or experiment test, allowing readers to test their codes at the beginning. To measure the accuracy of the proposed approach, the mean absolute percentage error (MAPE) between the prediction mean power and simulated mean power is calculated, which gives:

$$\mathrm{MAPE} = \frac{1}{M}\sum_{j=1}^{M}\left|\frac{\hat{\bar{P}}\left(x_j\right) - \bar{P}\left(x_j\right)}{\bar{P}\left(x_j\right)} \times 100\right| \tag{25}$$

where M is the total number of sea states, $\bar{P}\left(x_j\right)$ and $\hat{\bar{P}}\left(x_j\right)$ are respectively the simulated mean power and predicted mean power at the sea state x_j.

Table 1
ALK-PE approach for 1D analytic problem with different Φ values.

Approach	Simulation times	MAPE (%)	Efficiency increased (%)
Ref.	201	–	–
ALK-PE ($\Phi = 2$)	13	0.03	1546.15
ALK-PE ($\Phi = 5$)	13	0.03	1546.15
ALK-PE ($\Phi = 10$)	13	0.03	1546.15

3.4.1. One-dimensional analytic example

In the first example, the mean power $\overline{P}$ is considered as a function of variable x as given in the following equation.

$$\overline{P}(x) = x + xsin(x) \tag{26}$$

The x variable interval is from 1 to 11. A total of 201 samples ($M = 201$) are generated by grid sampling from x, and the simulated mean power (SMP) values are shown in Fig. 5(a). In this example, four initial samples ($mi = 4$) are generated to train the Kriging model at first. The initial training results and 95% confidence interval are given in Fig. 5(b). Need to mention in Fig. 5, "IDoEs" and "EDoEs" respectively represent the initial training points (also known as design of experiments) and enriched points. The initial prediction mean power (PMP) has a big difference compared with the simulated mean power. The MAPE values between SMP and PMP are even greater than 100%, as shown in Fig. 5(f). Then, the active learning approach starts to update the Kriging model by reducing the prediction error, as shown in Fig. 5(c) and (d). The MAPE values will decrease significantly. In the end, when the stopping criterion is satisfied ($\min(U) > \Phi$), the PMP is nearly the same as the SMP, and only 13 points are used to train the Kriging model as depicted in Fig. 5(e). Additionally, the results considering different Φ values are summarized in Table 1. As shown in the table, the proposed ALK-PE can efficiently and accurately estimate the simulated results. The efficiency can increase more than 15 times, and MAPE is less than 0.1%. Here the efficiency is calculated based on simulation times. However, due to the simplicity of this one-dimensional problem, the impact of Φ is not yet visible. To investigate the effect of Φ on the algorithm, another two-dimension problem is studied.

3.4.2. Two-dimensional analytic example

In the second example. it is considered that the mean power $\overline{P}$ is a function of variable x_1 and x_2 as shown in the following equation:

$$\overline{P}(x_1, x_2) = |x_1 sin(x_1) + x_2 cos(x_2) + 10| \tag{27}$$

where the x_1 variable interval is from 0 to 10, and the x_2 variable interval is from 0 to 5. The total samples and discretization of each variable are given in Table 2. Also, the initial data set is given in Table 2 and 12 initial samples ($mi = 12$) are used to construct the Kriging model at the beginning. The simulated mean power is given in Fig. 6(a). The initial Kriging prediction and the final prediction are respectively given in Fig. 6(b) and (c). In Fig. 6(b), the initial Kriging prediction can well capture the distribution of the mean power but remain a big difference in details. That is why the MAPE values are bigger than 30% at the beginning, as shown in Fig. 6(d). Then, the active learning process updates the Kriging model efficiently, and the MAPE values significantly drop. In the end, the Kriging model can accurately predict globally and locally. In addition, the results considering different Φ are also summarized in Table 3. As shown in Table 3, the value Φ will affect the efficiency and accuracy of the ALK-PE approach. With a bigger Φ value, the prediction accuracy will increase, but the efficiency will decrease. To compromise between the efficiency of the ALK-PE approach and the accuracy of the Kriging prediction, the Φ value equal to 5 is considered in the following section, which normally can ensure the MAPE is less than 5%.

4. WEC power matrix estimation by ALK-PE approach

This section applies the proposed approach to a point absorber WEC. A general flowchart of applying the proposed approach to WECs is shown in Fig. 7. At first, the Kriging model is trained with the initial sea state cases X_{doe} and the simulated mean power $\bar{P}_{doe}$. Then, the active learning process will select the sea state case with the maximum Kriging prediction error for the next simulation. The newly selected case x_{i*} and the simulated $\bar{P}_{i*}$ value are used to update the Kriging until the convergence criterion is satisfied. Two different cases are studied in this part. The first one considers that the maximum PTO force is not limited, and the second one considers that the maximum PTO force is limited to 80 kN. The typical wave states and the related initial training samples are given as shown in Table 4. In this section, the significant wave height H_s is considered between 0.5 and 6.5 m, and the wave peak period T_p is from 3 to 15 s. The interval of H_s and T_p are both equal to 0.5, which can be considered a good representation of most sea states. A total number of 325 sea-state cases is considered for the power matrix estimation, and only 16 sea-state cases are used to train the Kriging model initially. Regarding the simulated results of the WEC, the mean absorbed power and STD of the PTO force at each wave state are obtained by the spectral-domain model detailed in Section 2.2. Considering the purpose of this work, the numerical model is only intended to provide reference data, namely the power matrix, for demonstrating the performance of the proposed ALK-PE approach. The accuracy of the spectral-domain model in the power calculation of WECs has been verified in previous studies (Tan et al., 2022a, 2023b).

4.1. Power matrix of the WEC without PTO force constraint

In the first case, the maximum PTO force is not limited. The WEC power matrix is obtained by the spectral-domain model. The related STD of PTO force and the optimized PTO damping in each wave state is given in Fig. 8. The simulated mean power of the WEC and the ALK-PE approach prediction are depicted in Fig. 9. Fig. 8(a) depicts the simulated value of STD of the PTO force. The increased significant wave height results in larger WEC displacement and therefore higher velocity. Besides, as shown in Fig. 8(b), the optimized PTO damping clearly goes up with the peak period. Consequently, referring to Eq. (16) in mind, it is reasonable that STD of the PTO force increases with the significant wave height and peak period. Besides, it can be seen in Fig. 8(b) that the optimized PTO damping tends to be highly linear with regard to the peak period. This is because the tuning of the PTO damping is not constrained by the PTO force limit. In Fig. 9(a), the simulated mean absorbed power is presented. It can be seen that the absorbed power tends to increase with the significant wave height, because the increased significant wave height is associated with higher power input with the same peak period. Comparatively, the power absorption peaks up around the peak period of 7 s, which can be explained by the natural frequency of the WEC corresponding to the value. Furthermore, the nonlinearity of the system is insignificant. As a consequence, the estimated values of STD of PTO force and the mean power, as shown in Figs. 8(a) and 9(a), present a tendency of relatively mild variation between adjacent cases of wave states. Hence, this scenario can be regarded as a simple case. The results of the ALK-PE approach are also depicted in Fig. 9. As shown in Fig. 9(b), the initial prediction of the Kriging model can only capture the global trend of the distribution of the mean power. However, the prediction is not good in the local wave states, especially in the boundary wave state. That is why the MAPE values are much higher in the beginning. With the enrichment of the ALK-PE process, the MAPE values will decrease. In the end, the Kiring prediction can accurately predict the power matrix. The final results are given in Table 5. Trough ALK-PE approach, only 28 simulations are needed to obtain the power matrix of the WEC, which saves more than 10-time simulations. Also, the MAPE between simulated mean power and predicted mean power is less than 1%.

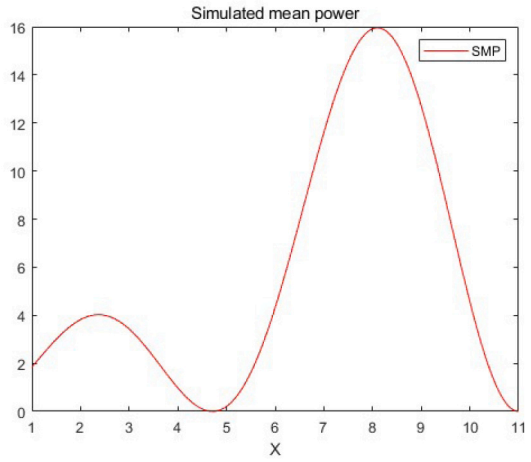

(a) Original mean power

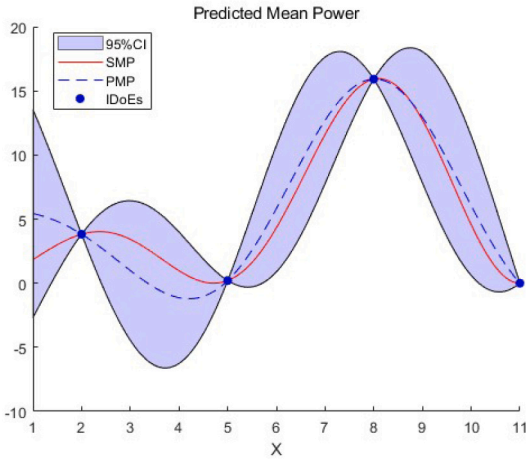

(b) Initial prediction

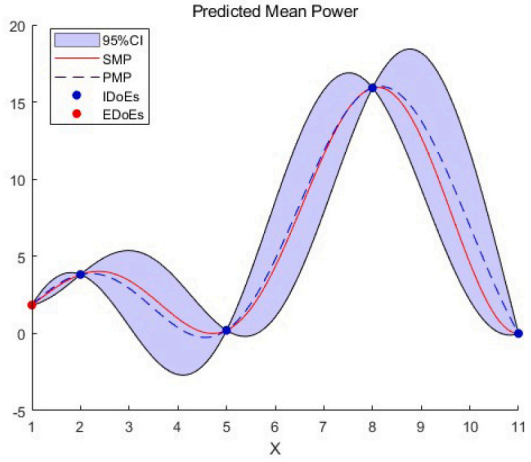

(c) The 1st enrichment

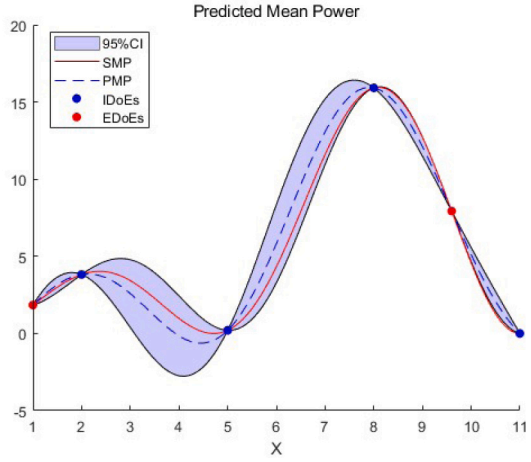

(d) The 2nd enrichment

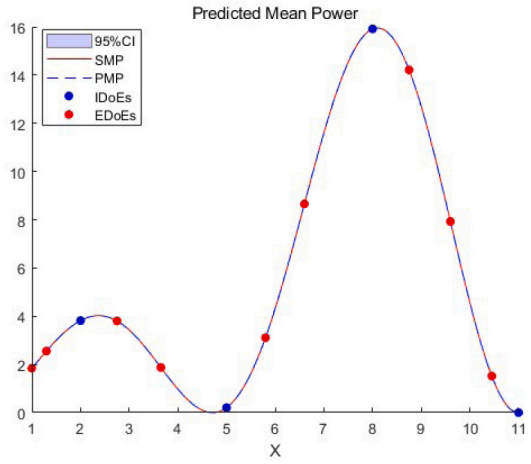

(e) Final prediction

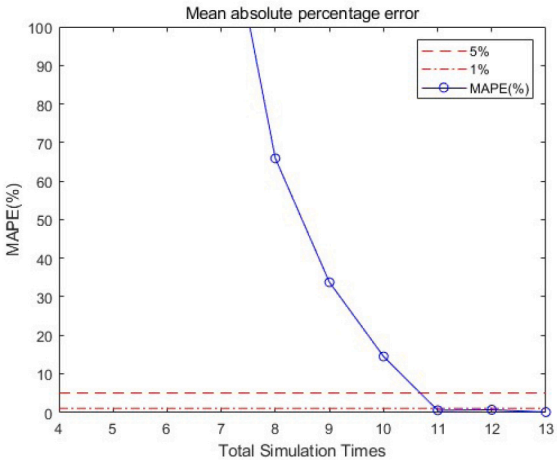

(f) Mean error between prediction and true value

Fig. 5. 1D analytic problem.

4.2. Power matrix of the WEC with PTO force constraint

In the second case, the PTO force is limited because, in reality, considering the cost and volume of the PTO system, the PTO system can only provide limited force. That will change the performance of WECs and also the power generation. The performance of WECs is also simulated based on the spectral-domain model. The related STD of PTO force and the optimized PTO damping are given in Fig. 10. As shown in Fig. 10, due to the limitation of the PTO force, STD of the force will reach the limit with the increase of wave height. Correspondingly, the implementation of the PTO force constraint also makes a difference in the optimization of PTO damping coefficients. It is visible in Fig. 10(b)

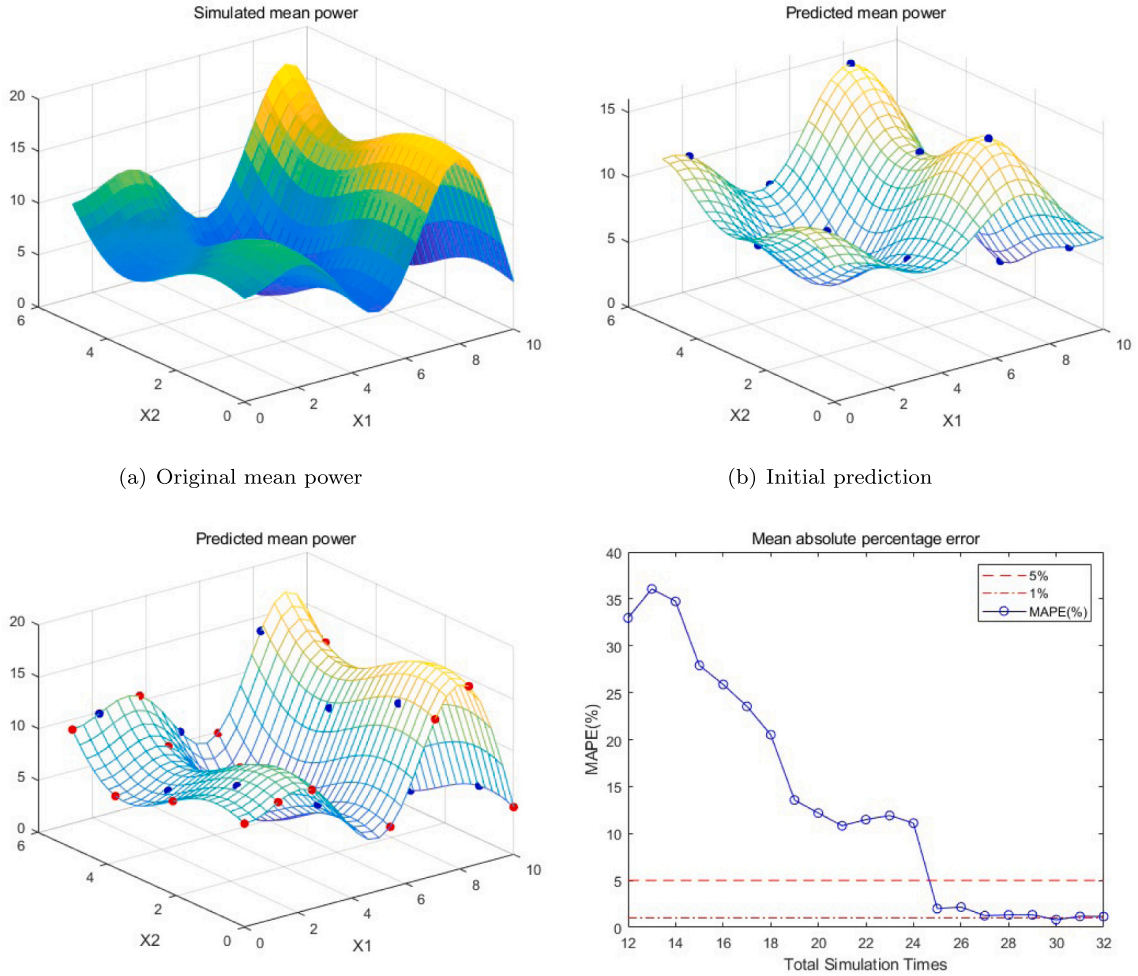

(a) Original mean power

(b) Initial prediction

(c) Final prediction

(d) Mean error between prediction and true value

Fig. 6. 2D problem.

Table 2
Parameter description of 2D analytic problem.

Parameter	Domain of variation	Discretization	Number of cases	Initial grid samples
x_1	[0, 10]	0.4	25	[1, 4, 7, 10]
x_2	[0, 5]	0.2	25	[1, 3, 5]
Total cases			$M = 625$	$mi = 12$

Table 3
ALK-PE approach for 2D analytic problem with different Φ values.

Approach	Simulation times	MAPE (%)	Efficiency increased (%)
Ref.	625	–	–
ALK-PE ($\Phi = 2$)	21	10.82	2976.19
ALK-PE ($\Phi = 5$)	26	2.16	2403.85
ALK-PE ($\Phi = 10$)	32	1.15	1953.13

that the optimized PTO damping sharply decreases after the wave height is higher than a certain value. This can be explained by the fact that the PTO force increases with the PTO damping coefficient. Subject to larger wave heights, the PTO damping of the WEC has to be reduced to comply with the defined PTO force constraints. Therefore, the nonlinearity of the WEC system is intensified when the PTO force constraint is taken into consideration. This is also noted in the estimation of the power matrix, as depicted in Fig. 11(a). In this sense, the difficulty of the second case for the ALK-PE approach is expected to be higher than that in the first case. The simulated mean power and ALK-PE approach prediction are given in Fig. 11. Similarly, at the start, the Kriging prediction is not accurate but with the enrichment of the active learning process, the final prediction can predict well the mean power at each wave state. The final results are summarized in Table 6. Even though the limited PTO force increases the complexity of the problem, the proposed approach can also accurately predict the mean power with less computational cost. Only 59 simulations are required to predict all the wave states and the mean errors are around 1%, which saves more than 5-time simulations.

5. Conclusion and discussion

In this paper, an active learning Kriging approach named ALK-PE is proposed to estimate the WEC power matrix with less computational cost. At first, the concept of the considered WEC is described and the derivation of the numerical model used to predict the dynamics of the WEC is presented. Then, the basic idea of active learning strategies

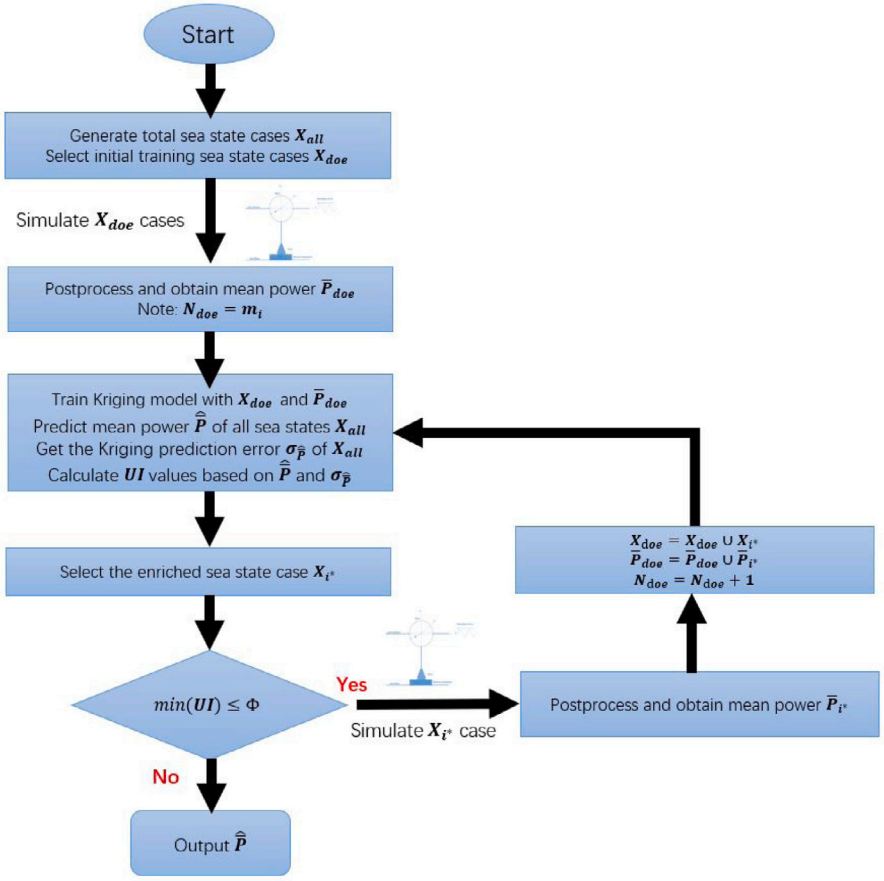

Fig. 7. General flowchart of the ALK-PE approach application for WECs.

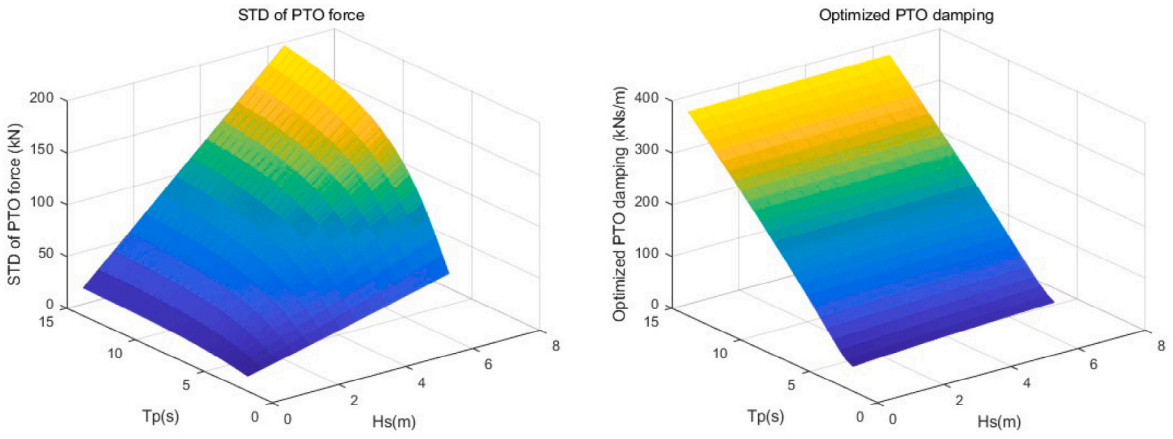

(a) STD of PTO force (b) Optimized PTO damping

Fig. 8. STD of PTO force and optimized PTO damping without PTO force constraint.

Table 4
Typical sea state cases and initial training cases.

Parameter	Domain of variation	Discretization	Number of cases	Initial grid samples
H_s (m)	[0.5, 6.5]	0.5	13	[1, 2.5, 4, 5.5]
T_p (s)	[3, 15]	0.5	25	[3.5, 6.5, 9.5, 12.5]
Total cases			$M = 325$	$mi = 16$

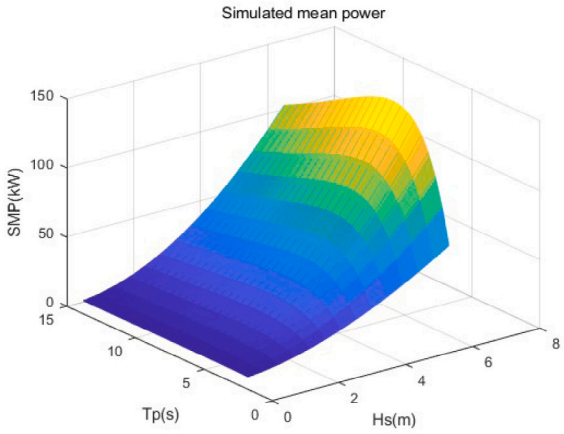

(a) Simulated mean power

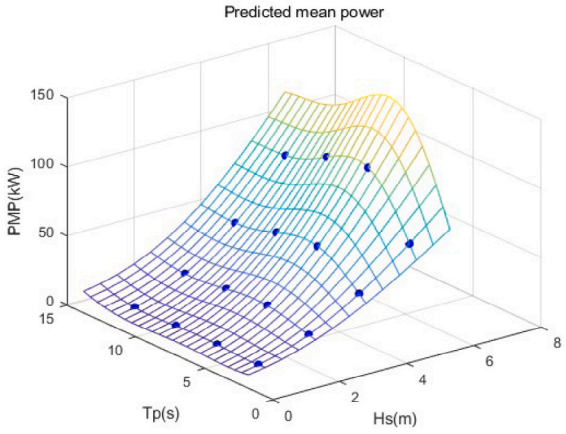

(b) Initial prediction

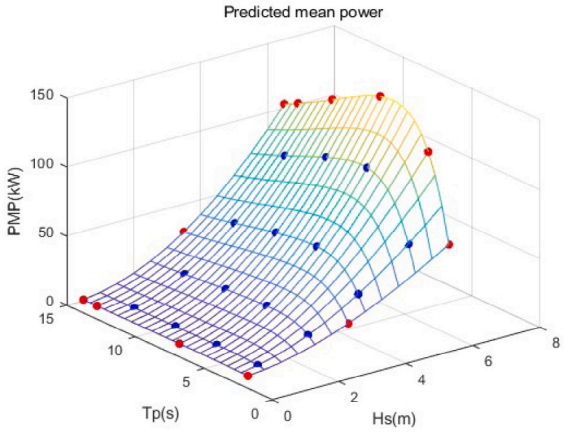

(c) The final prediction

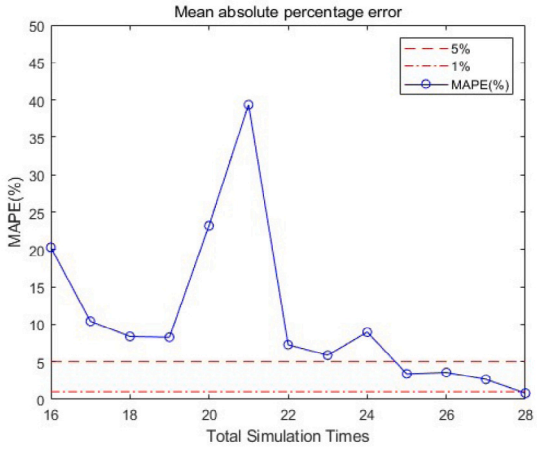

(d) MAPE convergence plot

Fig. 9. WEC power matrix prediction without PTO force constraint.

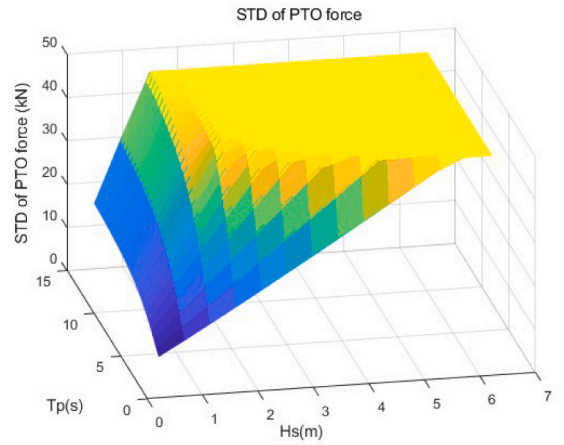

(a) STD of PTO force

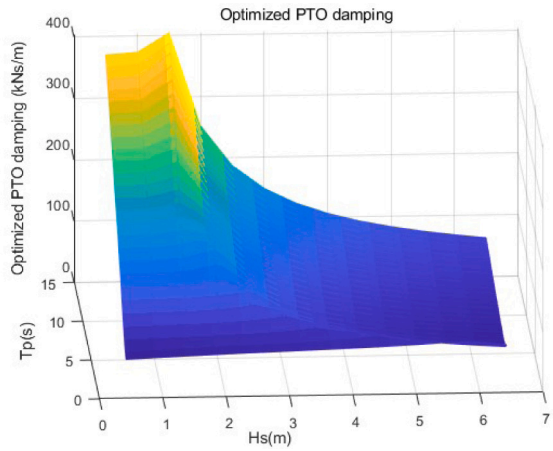

(b) Optimized PTO damping

Fig. 10. STD of PTO force and optimized PTO damping.

is introduced. The learning function and stopping criterion of ALK-PE are presented. Two analytic examples are used to demonstrate the efficiency and accuracy of the proposed ALK-PE. The threshold of the stopping condition is also studied. Finally, the proposed approach is applied to a point absorber WEC. Two different cases are considered in the point absorber. The results show:

The proposed approach can efficiently and accurately estimate the power matrix of the WEC. The efficiency can increase by about 11 times in the unlimited PTO force case, and the MAPE between SMP and PMP is about 1%. In the second case, although the nonlinearity of the mean power estimation increase with the limitation of PTO force, the proposed approach can also use less than one-fifth of the

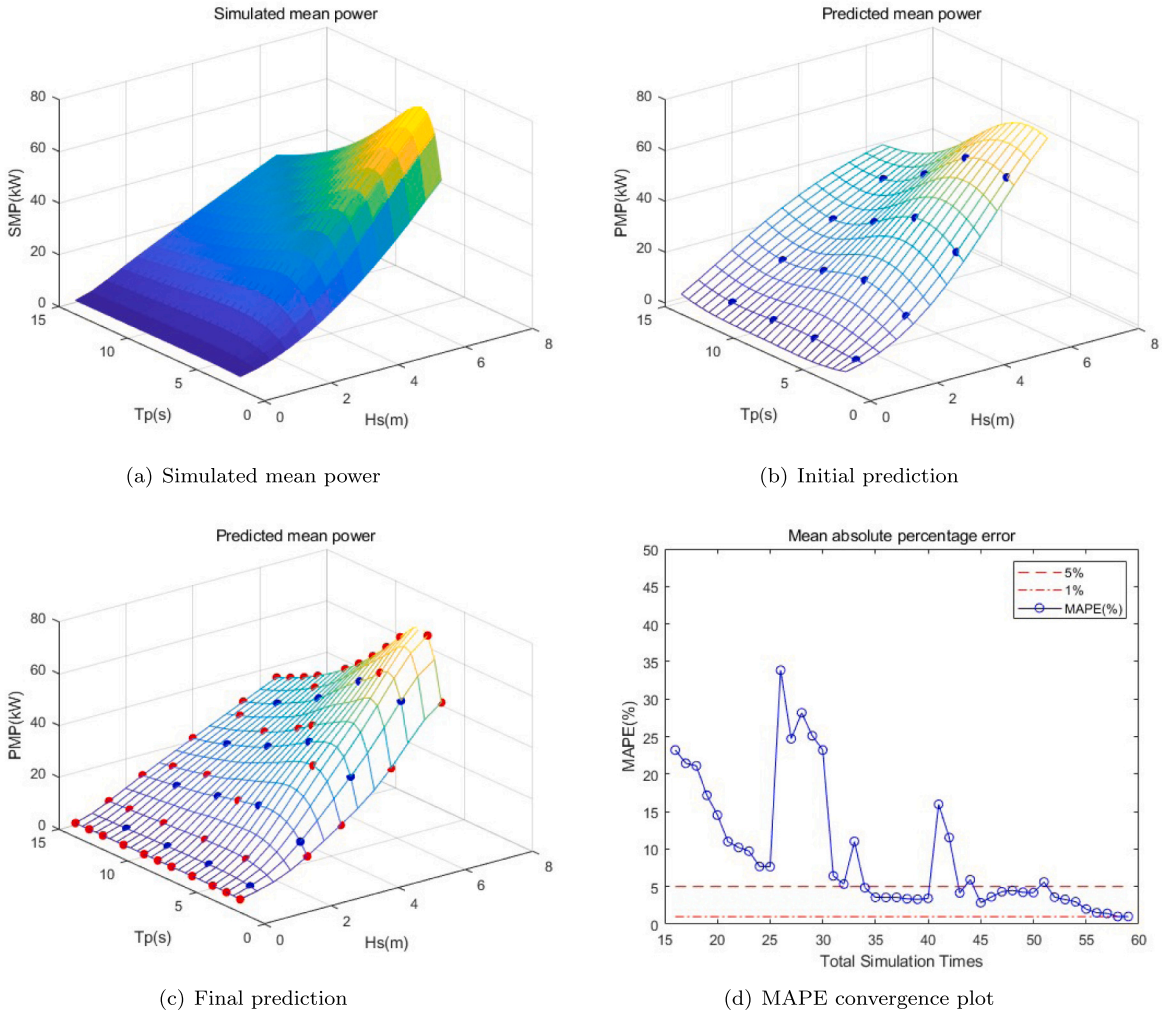

(a) Simulated mean power

(b) Initial prediction

(c) Final prediction

(d) MAPE convergence plot

Fig. 11. WEC power matrix prediction with PTO force limit.

Table 5
ALK-PE approach for a point absorber WEC without PTO force limit.

Approach	Simulation times	MAPE (%)	Efficiency increased (%)
Ref.	325	–	–
ALK-PE ($\Phi = 5$)	28	0.80	1160.71

Table 6
ALK-PE approach for a point absorber WEC with PTO force limit.

Approach	Simulation times	MAPE (%)	Efficiency increased (%)
Ref.	325	–	–
ALK-PE ($\Phi = 5$)	59	1.02	550.85

simulations to predict the whole power matrix and keep MAPE values around 1%. In both two cases, more than 5-time simulations are saved. The ALK-PE approach will save computational or experimental resources when estimating the power matrix by means of time-domain modeling or physical experiments. Given the current state of wave energy converters, achieving large-scale commercialization would involve numerous iterations to fine-tune design parameters. The proposed approach, thanks to its combined high efficiency and accuracy, is anticipated to significantly enhance this optimization process.

In the future, the proposed approach will apply the other types of wave connectors, e.g., the overtopping devices and oscillating water columns. Also, need to mention; the proposed approach is not only suitable for the mean power matrix estimation but also can be extended to other WECs' performance estimations, e.g., optimized PTO damping estimation. Furthermore, only a single WEC is considered in the present work. However, for economic consideration, WECs are expected to appear in the form of wave farms in which plenty of WECs are operating in one region collectively. The performance identification of wave farms would be much more complicated than that for a single WEC because of the interaction between devices. Then, relying on traditional numerical models, the optimization of the farm layout and device shape could be extremely time-demanding. In that sense, the application of the ALK-PE method could significantly accelerate the development of WECs.

CRediT authorship contribution statement

Chao Ren: Conception and design of study, Acquisition of data, Analysis and/or interpretation of data, Writing – original draft, Writing – review & editing. **Jian Tan:** Conception and design of study, Acquisition of data, Analysis and/or interpretation of data, Writing – original draft, Writing – review & editing. **Yihan Xing:** Conception and design of study, Acquisition of data, Analysis and/or interpretation of data, Writing – original draft, Writing – review & editing.

Declaration of competing interest

The authors declare that they have no known competing financial interests or personal relationships that could have appeared to influence the work reported in this paper.

Data availability

Data will be made available on request.

Acknowledgment

All authors approved the version of the manuscript to be published.

References

Antonio, F. de O., 2010. Wave energy utilization: A review of the technologies. Renew. Sustain. Energy Rev. 14 (3), 899–918.

Astariz, Sharay, Iglesias, Gregório, 2015. The economics of wave energy: A review. Renew. Sustain. Energy Rev. 45, 397–408.

Bento, PMR, Pombo, JAN, Mendes, RPG, Calado, MRA, Mariano, SJPS, 2021. Ocean wave energy forecasting using optimised deep learning neural networks. Ocean Eng. 219, 108372.

De Andres, Adrian, Maillet, Jéromine, Hals Todalshaug, Jørgen, Möller, Patrik, Bould, David, Jeffrey, Henry, 2016. Techno-economic related metrics for a wave energy converters feasibility assessment. Sustainability 8 (11), 1109.

De Andres, A., Medina-Lopez, E., Crooks, D., Roberts, O., Jeffrey, H., 2017. On the reversed LCOE calculation: Design constraints for wave energy commercialization. Int. J. Mar. Energy 18, 88–108.

Echard, Benjamin, Gayton, Nicolas, Lemaire, Maurice, 2011. AK-MCS: an active learning reliability method combining Kriging and Monte Carlo simulation. Struct. Saf. 33 (2), 145–154.

Edition, First, Journée, J.M.J., Massie, W.W., 2001. Offshore Hydromechanics. Delft University of Technology.

Folley, Matt, 2016. Numerical Modelling of Wave Energy Converters: State-of-the-Art Techniques for Single Devices and Arrays. Academic Press.

Folley, Matt, Babarit, Aurélien, Child, Ben, Forehand, David, O'Boyle, Louise, Silverthorne, Katie, Spinneken, Johannes, Stratigaki, Vasiliki, Troch, Peter, 2012. A review of numerical modelling of wave energy converter arrays. In: International Conference on Offshore Mechanics and Arctic Engineering, Vol. 44946. American Society of Mechanical Engineers, pp. 535–545.

Folley, Matt, Whittaker, Trevor, 2010. Spectral modelling of wave energy converters. Coast. Eng. 57 (10), 892–897.

Folley, Matt, Whittaker, Trevor, 2013. Validating a spectral-domain model of an OWC using physical model data. Int. J. Mar. Energy 2, 1–11.

Giorgi, Giuseppe, Ringwood, John V., 2017. Consistency of viscous drag identification tests for wave energy applications. In: 12th European Wave and Tidal Energy Conference. pp. 1–8.

Hadi, Behnaz, Khosravi, Alireza, Sarhadi, Pouria, 2022. Deep reinforcement learning for adaptive path planning and control of an autonomous underwater vehicle. Appl. Ocean Res. 129, 103326.

Journée, J.M.J., Massie, W.W., Huijsmans, R.H.M., 2015. Offshore hydrodynamics.

Krige, Daniel G., 1951. A statistical approach to some basic mine valuation problems on the Witwatersrand. J. South. Afr. Inst. Min. Metall. 52 (6), 119–139.

Lophaven, Søren N, Nielsen, Hans Bruun, Sondergaard, Jacob, Dace, A, 2002. A Matlab Kriging Toolbox. Technical University of Denmark Report IMM-TR-2002-12, Citeseer.

Lu, Hongfang, Xi, Dongmin, Ma, Xin, Zheng, Saina, Huang, Cheng, Wei, Nan, 2022. Hybrid machine learning models for predicting short-term wave energy flux. Ocean Eng. 264, 112258.

Mérigaud, Alexis, Ringwood, John V., 2017. A nonlinear frequency-domain approach for numerical simulation of wave energy converters. IEEE Trans. Sustain. Energy 9 (1), 86–94.

Moustapha, Maliki, Marelli, Stefano, Sudret, Bruno, 2022. Active learning for structural reliability: Survey, general framework and benchmark. Struct. Saf. 96, 102174.

Nielsen, Kim, Wendt, Fabian, Yu, Yi-Hsiang, Ruehl, Kelley, Touzon, Imanol, Nam, Bo Woo, Kim, Jeong Seok, Kim, Kyong-Hwan, Crowley, Sarah, Sheng, Wanan, et al., 2018. OES task 10 WEC heaving sphere performance modelling verification. In: Advances in Renewable Energies Offshore, Proceedings of the 3rd International Conference on Renewable Energies Offshore (RENEW 2018), Lisbon, Portugal, 8–10 October 2018. CRC Press London, UK, pp. 265–273.

O'connor, M., Lewis, T., Dalton, G., 2013. Techno-economic performance of the Pelamis P1 and Wavestar at different ratings and various locations in Europe. Renew. energy 50, 889–900.

Pedregosa, F., Varoquaux, G., Gramfort, A., Michel, V., Thirion, B., Grisel, O., Blondel, M., Prettenhofer, P., Weiss, R., Dubourg, V., Vanderplas, J., Passos, A., Cournapeau, D., Brucher, M., Perrot, M., Duchesnay, E., 2011. Scikit-learn: Machine learning in python. J. Mach. Learn. Res. 12, 2825–2830.

Penalba Retes, Markel, Giorgi, Giuseppe, Ringwood, John, 2015. A review of non-linear approaches for wave energy converter modelling. In: Proceedings of the 11th European Wave and Tidal Energy Conference. European Wave and Tidal Energy Conference 2015.

Ren, Chao, 2022. Reliability Assessment of an Offshore Wind Turbine Jacket with Active Learning Approaches (Ph.D. thesis). Normandie Université.

Ren, Chao, Aoues, Younes, Lemosse, Didier, De Cursi, Eduardo Souza, 2020. Structural reliability assessment of offshore wind turbine jacket considering corrosion degradation.

Ren, Chao, Aoues, Younes, Lemosse, Didier, De Cursi, Eduardo Souza, 2022. Ensemble of surrogates combining Kriging and Artificial Neural Networks for reliability analysis with local goodness measurement. Struct. Saf. 96, 102186.

Ren, Chao, Aoues, Younes, Lemosse, Didier, De Cursi, Eduardo Souza, 2023. Reliability assessment of an offshore wind turbine jacket under one ultimate limit state considering stress concentration with active learning approaches. Ocean Eng. 281, 114657.

Ren, Chao, Xing, Yihan, 2023. AK-MDAmax: Maximum fatigue damage assessment of wind turbine towers considering multi-location with an active learning approach. Renew. Energy 118977.

Roberts, Owain, Jeffrey, Henry, MacGillivray, Andy, Guanche, Raul, de Andres, Adrian, 2016. Beyond LCOE: A study of ocean energy technology development and deployment attractiveness. Sustain. Energy Technol. Assess. 19, 1–16.

Sarkar, Dripta, Contal, Emile, Vayatis, Nicolas, Dias, Frederic, 2016. Prediction and optimization of wave energy converter arrays using a machine learning approach. Renew. Energy 97, 504–517.

Settles, Burr, 2009. Active learning literature survey.

Stetco, Adrian, Dinmohammadi, Fateme, Zhao, Xingyu, Robu, Valentin, Flynn, David, Barnes, Mike, Keane, John, Nenadic, Goran, 2019. Machine learning methods for wind turbine condition monitoring: A review. Renew. Energy 133, 620–635.

Suchithra, R., Ezhilsabareesh, K., Samad, Abdus, 2019. Development of a reduced order wave to wire model of an OWC wave energy converter for control system analysis. Ocean Eng. 172, 614–628.

Tan, Jian, Polinder, Henk, Laguna, Antonio Jarquin, Miedema, Sape, 2022a. The application of the spectral domain modeling to the power take-off sizing of heaving wave energy converters. Appl. Ocean Res. 122, 103110.

Tan, Jian, Polinder, Henk, Laguna, Antonio Jarquin, Miedema, Sape, 2022b. A numerical study on the performance of the point absorber Wave Energy Converter integrated with an adjustable draft system. Ocean Eng. 254, 111347.

Tan, Jian, Polinder, Henk, Laguna, Antonio Jarquin, Miedema, Sape, 2023a. A wave-to-wire analysis of the adjustable draft point absorber wave energy converter coupled with a linear permanent-magnet generator. Ocean Eng. 276, 114195.

Tan, Jian, Polinder, Henk, Laguna, Antonio Jarquin, Wellens, Peter, Miedema, Sape A, 2021. The influence of sizing of wave energy converters on the techno-economic performance. J. Mar. Sci. Eng. 9 (1), 52.

Tan, J., Polinder, H., Wellens, P., Miedema, S., 2020. A feasibility study on downsizing of power take off system of wave energy converters. Dev Renew Energies Offshore 140–148.

Tan, Jian, Tao, Wei, Laguna, Antonio Jarquin, Polinder, Henk, Xing, Yihan, Miedema, Sape, 2023b. A spectral-domain wave-to-wire model of wave energy converters. Appl. Ocean Res. 138, 103650.

Tan, Jian, Wang, Xuezhou, Polinder, Henk, Laguna, Antonio Jarquin, Miedema, Sape A, 2022c. Downsizing the linear PM generator in wave energy conversion for improved economic feasibility. J. Mar. Sci. Eng. 10 (9), 1316.

Wei, Yanji, Bechlenberg, Alva, van Rooij, Marijn, Jayawardhana, Bayu, Vakis, Antonis I, 2019. Modelling of a wave energy converter array with a nonlinear power take-off system in the frequency domain. Appl. Ocean Res. 90, 101824.

Zhou, Huanyu, Qiu, Yingning, Feng, Yanhui, Liu, Jing, 2022. Power prediction of wind turbine in the wake using hybrid physical process and machine learning models. Renew. Energy 198, 568–586.

Zhu, Kai, Shi, Hongda, Han, Meng, Cao, Feifei, 2022. Layout study of wave energy converter arrays by an artificial neural network and adaptive genetic algorithm. Ocean Eng. 260, 112072.